

Radiative Models of Sagittarius A* and M87 from Relativistic MHD Simulations

J. Dexter¹, E. Agol², P. C. Fragile³ and J. C. McKinney⁴

¹Theoretical Astrophysics Center and Department of Astronomy, University of California, Berkeley, CA 94720-3411, USA

²Department of Astronomy, University of Washington, Box 351580, Seattle, WA 98195, USA

³Department of Physics & Astronomy, College of Charleston, Charleston, SC 29424, USA

⁴Kavli Institute for Particle Astrophysics and Cosmology, Stanford University, Stanford, CA 94305-4060, USA

E-mail: jdexter@berkeley.edu

Abstract. Ongoing millimeter VLBI observations with the Event Horizon Telescope allow unprecedented study of the innermost portion of black hole accretion flows. Interpreting the observations requires relativistic, time-dependent physical modeling. We discuss the comparison of radiative transfer calculations from general relativistic MHD simulations of Sagittarius A* and M87 with current and future mm-VLBI observations. This comparison allows estimates of the viewing geometry and physical conditions of the Sgr A* accretion flow. The viewing geometry for M87 is already constrained from observations of its large-scale jet, but, unlike Sgr A*, there is no consensus for its millimeter emission geometry or electron population. Despite this uncertainty, as long as the emission region is compact, robust predictions for the size of its jet launching region can be made. For both sources, the black hole shadow may be detected with future observations including ALMA and/or the LMT, which would constitute the first direct evidence for a black hole event horizon.

1. Introduction

The Galactic center massive black hole candidate, Sagittarius A* (Sgr A*) [1], and the supermassive black hole candidate in the center of M87 are both bright radio sources and are the two largest black holes in angular size (4 – 5 microarcseconds or μas). For both these reasons, they are the two major targets of interest for imaging with ongoing very long baseline interferometry observations at millimeter wavelengths (mm-VLBI), which have already detected time-variable event horizon scale structure in Sgr A* [2, 3]. Data have also been taken for M87, but are as yet unpublished. The Sgr A* data have previously been fit both with simple geometric models (symmetric Gaussian and annulus of constant brightness) and using a radiatively inefficient accretion flow model (RIAF, [4, 5, 6]). While physically motivated, these models are non-relativistic and do not include the magnetic fields that drive turbulence in the accretion flow via the magnetorotational instability (MRI, [7]), causing accretion and leading to the observed synchrotron radiation.

This essential physics can now be captured in general relativistic MHD (GRMHD) simulations of black hole accretion. Simulations have been used to model the millimeter emission in Sgr A* either in the absence of general relativity [8] or in axisymmetry [9, 10, 11]. The millimeter

emission in the models arises in the innermost portions of the accretion flow ($r \simeq 5M$, where we use $G = c = 1$ units except where otherwise noted), so that relativistic effects are dominant. In simulations run in axisymmetry, the MRI decays on the local orbital timescale. This leads to unrealistic variability, prevents the disk from reaching quasi-steady state, and can cause the appearance of unphysically hot and bright regions [10]. One group [11] has used 3D GRMHD simulations, but then time-averaged the resulting data. Two groups have compared spectra from 2D GRMHD simulations with the spectrum of M87 [12, 13], but neither considered jet emission or made predictions for mm-VLBI.

Here we discuss radiative models of the mm emission from Sgr A* and M87 for comparison with mm-VLBI constructed by performing relativistic radiative transfer calculations on 3D GRMHD simulation data. These are the first models to self-consistently include variability, and the M87 models are the first predictions for images of a jet launching region from a simulation. The numerical models of Sgr A* are the only ones to have been fit directly to mm-VLBI data to test GRMHD accretion theory and estimate parameters of the black hole and its accretion flow.

2. Radiative Modeling

A radiative model of Sagittarius A* or M87 consists of three components [14]: a dynamical solution for the fluid variables in the accretion flow, a model for the electron distribution function based on the dynamical solution, and an emission model given the electron distribution function. These components give fluid frame emission/absorption coefficients everywhere in spacetime. Observables are calculated from these coefficients in full general relativity via ray tracing [15].

2.1. GRMHD Simulations

The dynamical solution consists of the output of general relativistic MHD simulations of black hole accretion flows. The simulations start from a gas torus in hydrostatic equilibrium in a Kerr spacetime threaded with a weak magnetic field. This configuration quickly develops turbulence driven by the MRI, and the resulting stresses cause angular momentum transport outwards allowing accretion onto the black hole. These simulations are currently limited in several important respects: they only develop a quasi-steady accretion flow over a limited radial domain ($r \lesssim 25M$); and they neglect both the radiation that astronomers observe and the electrons that produce it.

In highly underluminous systems like Sgr A* and M87, ignoring the effects of radiation on the dynamical solution is reasonable (but see [16] and Dibi et al., in prep.). The limited radial domain is also acceptable given the extremely compact size measured by mm-VLBI, and found theoretically for the millimeter emission in Sgr A* and M87.

However, there are also issues with modeling these sources using GRMHD simulations. Their low densities means that the ions and electrons may have significantly different temperatures, with the hot ions providing the fluid pressure captured by the simulation and the cool electrons producing the observed emission. We must then decide how to model the electrons before calculating observables from simulation data (see § 2.2).

In this work, we consider results from four GRMHD simulations (summarized in Table 1 of [17]). All are three dimensional: in axisymmetry, the MRI decays on the local orbital timescale, preventing the accretion flow from reaching quasi-steady state and leading to artificial variability, an inaccurate time-averaged structure, and causing contamination of the spectra by unrealistically hot zones in the “funnel wall” [10]. The simulations are from two codes: `Cosmos++` [18, 19, 20] and a 3D extension of `HARM` [21, 22, 23, 24, 25]. The set of simulations is limited by the number of existing and available 3D GRMHD simulations of relatively thick ($H/R \simeq 0.2$) black hole accretion flows. The scarcity of simulations and their systematic differences prevent an estimate of the black hole spin. Only the MBD simulation forms a relativistic, magnetically dominated-jet and so this is the only simulation used in the disk/jet modeling of M87. We

use the last 2000 – 4000M of simulation data, once transients from the initial conditions have decayed, where 1M is 20s (9hr), 6×10^{11} cm (10^{15} cm), and $5\mu\text{as}$ ($4\mu\text{as}$) for Sgr A* (M87).

2.2. Electrons

The millimeter emission in Sgr A* is well described by synchrotron emission from hot, thermal electrons in the innermost portions of a radiatively inefficient accretion flow [26, 4]. A non-thermal tail extending to higher energies may be responsible for the radio and IR emission [4], or it may arise in a jet [27].

Since we focus on the millimeter emission, we model accretion disk components as having entirely thermal electrons. The electron temperature is specified using a constant electron-ion temperature ratio, T_i/T_e [8, 10], which allows the electron temperature to be calculated from the simulation pressure and density. This is the simplest possible prescription for a two-temperature accretion flow from a single fluid simulation.

In M87, it is unclear whether disk or jet emission is dominant at millimeter wavelengths. Extended jet structure is observed at 7mm [28, 29], indicating that the jet emission is at least comparable to that from the disk. Since in the simulations the jet forms self-consistently from an accretion flow, we include both disk and jet components with different assumed electron populations [30].

The ultrarelativistic outflow in the simulation forms in magnetically-dominated region, so to separate the regions for electron modeling we define the jet by $b^2/\rho c^2 > 1$, where b is the magnetic field strength and ρ is the fluid density. The jet electrons are assumed to be entirely non-thermal with a power law distribution. The simulation variables of density and internal energy (pressure) within magnetically-dominated regions are unreliable, since they are set by the artificial numerical floor values used for code stability. We therefore scale the non-thermal particle density with the only reliable simulation variable in the jet region, the magnetic energy density: $n_{\text{nth}} \propto b^2$, where n_{nth} is the non-thermal particle density (cf. [31]). Fitting the M87 spectrum requires 5 – 10% of the magnetic energy to be dissipated in non-thermal particles for the simulation considered.

In both cases, the emissivity is assumed to be entirely synchrotron radiation. Inverse Compton scattering is ignored, although it is likely to be very important for M87 at high energies [12, 30]. For the thermal disk electrons, we use an approximate form of the synchrotron emissivity given by Leung et al. (2011) [32]. For the jet power law electron distribution, we use a form of the emissivity that takes into account the low-energy cutoff to the distribution, which is important for the millimeter emission in M87 [14].

2.3. Ray Tracing

Relativistic radiative transfer is performed on the simulation data via ray tracing using the code `grtrans` [14]. Starting from an observer’s camera, rays are traced backwards in time toward the black hole assuming they are null geodesics (geometric optics approximation), using the public code `geokerr` [33]. In the region where rays intersect the accretion flow, the radiative transfer equation is solved along the geodesic, which then represents a pixel of the image. This procedure is repeated for many rays to produce an image, and at many time steps of the simulation to produce time-dependent images (movies). Light curves are computed by integrating over the individual images. Repeating the procedure over observed wavelengths gives a time-dependent spectrum.

To calculate fluid properties at each point on a ray, the spacetime coordinates of the geodesic are transformed from Boyer-Lindquist to the regular [34] or modified [35] Kerr-Schild coordinates used in the simulation. Since the accretion flow is dynamic, light travel time delays along the geodesic are taken into account. Data from the sixteen nearest zone centres (eight on the simulation grid over two time steps) are interpolated to each point on the geodesic.

Computing emission and absorption coefficients requires converting simulation fluid variables (pressure/internal energy, mass density, and magnetic field strength) into an electron distribution function in physical units. The black hole mass sets the length and time scales, while the mass of the initial torus provides an independent scale and fixes the accretion rate. The scalings are such that n and b^2 are proportional to the accretion rate.

3. Model Fitting

For Sgr A*, we fit simulated images at 1.3mm to mm-VLBI observations [2, 3] and the total flux at 1.3mm and 0.4mm to observations of the sub-mm spectral index [36]. Details on the statistical techniques used to estimate parameters from the fits can be found in [5, 17]. The free parameters for the Sgr A* models are i) the time-averaged accretion rate, ii) the ratio T_i/T_e , iii) the inclination and iv) sky orientation angles, and v) the simulation.

Generically, the simulated images provide excellent fits to the mm-wavelength observations of Sgr A* (reduced $\chi^2 \lesssim 1$ for many models for each simulation [37, 17]). Probability distributions for the inclination (i) and sky orientation (ξ) angles, the median electron temperature in the region that produces 99% of the millimeter emission (T_e), and the time-averaged accretion rate onto the black hole (\dot{M}) including all mm-VLBI data are estimated as follows (all to 90% confidence): $i = 60 \pm 15^\circ$, $\xi = -70^{+86}_{-15}^\circ$, $T_e = 6 \pm 2 \times 10^{10}\text{K}$ and $\dot{M} = 3^{+7}_{-1} \times 10^{-9} M_\odot \text{yr}^{-1}$. Including all of the data gives tighter constraints, but consistent estimates, for all parameters as found from the first epoch alone. The viewing angle estimates and probability distributions are in excellent agreement with those from using a RIAF model [5, 6]. The mm-VLBI observations, even with limited array coverage and sensitivity, are meaningfully constraining the relevant parameters, but they cannot yet distinguish between physical accretion flow models (they are, however, beginning to favor physical models over simple geometric ones [6]). The constraints on the accretion rate and electron temperature are consistent with, but independent of, estimates from the observed linear polarization and Faraday rotation measures [38, 39, 40] and spectral fitting [4], respectively.

The first mm-VLBI data for M87 have been obtained [3] but have not yet been published. We fit models to multi-epoch observational data in the optical [41], IR [42, 43], and mm [44], inflating the error bars to account for variability between the non-simultaneous observations and treating data points that may be dominated by dust in the galactic nucleus or large-scale jet emission as upper limits. Since there are roughly the same number of free parameters in the disk/jet models as spectral constraints, we identify fiducial models rather than attempt to quantitatively constrain the parameters. The models can be either disk/jet (DJ1) or jet only (J2), and provide satisfactory descriptions of the emission from the immediate vicinity of the M87 black hole [30].

The viewing geometry of M87, unlike Sgr A*, may be constrained by the Lorentz factor and sky orientation of the large-scale jet, which can reasonably be assumed to correspond to the black hole spin axis. All models assume this favored geometry ($i < 40^\circ$, $-115^\circ < \xi < -75^\circ$).

4. Black Hole Images

The millimeter emission from Sgr A* and M87 arises from the immediate vicinity of the black hole ($r < 5 - 10\text{M}$ for disk and $r < 2 - 4\text{M}$ for jet emission). On these scales, relativistic effects tend to dominate the appearance of the images, provided that the emission region is not completely optically thick. The important effects are: i) Doppler beaming from the component of the fluid velocity along the observer's line of sight, which is significant except for face-on viewing, and dominant for edge-on viewing; ii) light bending, which causes the back of the accretion flow to appear above/below the black hole (again except for face-on viewing), and iii) gravitational lensing. Doppler beaming causes significant asymmetry between the sides of the image where the gas is moving towards and away from the observer. The combination of ii)

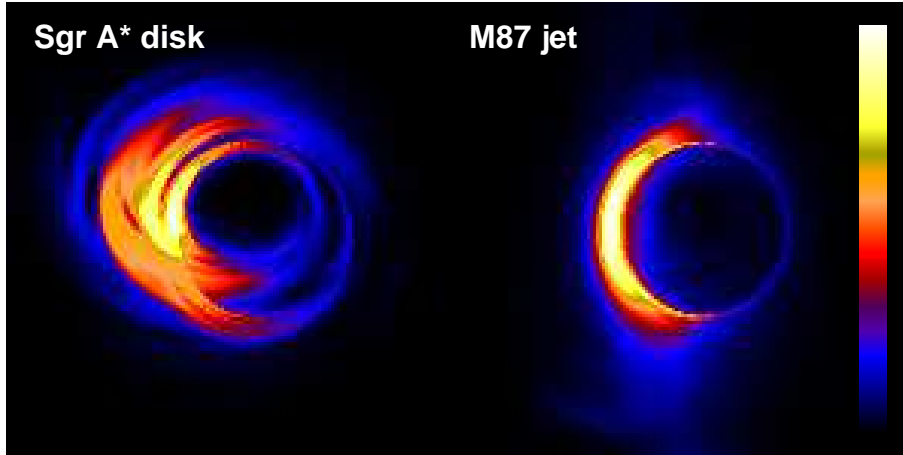


Figure 1. False color fiducial images of an accretion disk model of Sgr A* (left) and a jet image of M87 (right). The left/right asymmetries are caused by Doppler beaming from orbital motion, and the black hole shadow is clearly visible in the center of both images. The intensity scale is linear with a dynamic range of 60, and the panels are each 12 Schwarzschild radii ($\simeq 100$ microarcseconds) across.

and iii) importantly leads to the black hole “shadow” [45, 46, 17], the transition between bound and unbound photon orbits. For lines of sight inside the shadow, the emission comes from in front of the black hole, where few photon emission angles escape to the observer at infinity. The gravitational lensing in the immediate vicinity often leads to a bright ring at the circular photon orbit, surrounding the shadow. Observing signatures of this shadow would constitute the first direct evidence for a black hole event horizon. The combined effects of asymmetry from Doppler beaming and light bending are typically both important for favored models of M87 and Sgr A*, leading to characteristic crescent image morphologies (an example is shown in the left panel of Figure 1). The shadow is also apparent in the image.

4.1. The Size of M87

For the low inclination of M87, both disk and jet models also lead to crescent images. In the jet case, the emission arises in the *counter-jet*, since the emission from the forward jet is along lines of sight in the shadow and very little of it reaches the observer (see the right panel of Figure 1 for an example). For this reason, we can robustly predict the size of the jet launching region despite significant model uncertainties, as long as the emission region is compact ($r \lesssim 10M$) and not completely opaque ($\tau \lesssim 3$). We also assume the viewing geometry estimated from observations of the large-scale jet.

We predict the size observed by mm-VLBI by interpolating fiducial images to the locations sampled by the current mm-VLBI array [3]. The results are $\simeq 33 - 44 \mu\text{as}$, or 4–5 Schwarzschild radii [30], very similar to existing observations of Sgr A*.

4.2. Black Hole Shadow

Best fit models of Sgr A* and fiducial jet or disk/jet models of M87 all lead to crescent images, where Doppler beaming leads to significant asymmetry but the front and back of the accretion flow lead to significant contrast above and below the black hole. The black hole shadow is then visible on orientations probing the front/back of the accretion flow, while the image appears roughly Gaussian on baselines probing orientations that are significantly affected by

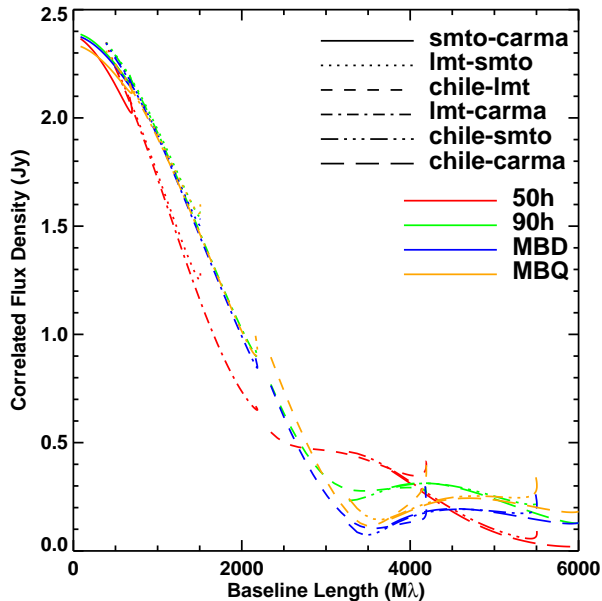


Figure 2. Visibility amplitude (Fourier transform of image intensity) as a function of baseline length for best fit models from [17] at 1.3mm. The telescopes considered are in Arizona (SMTO), California (CARMA), Mexico (LMT) and Chile (APEX/ASTE/ALMA). The BH shadow appears as the local minimum near 3000M λ on the LMT-Chile and Chile-CARMA baselines.

Doppler beaming. For both sources, the models predict that the black hole shadow is not visible with current telescopes (roughly East-West baselines), but may be observed with North-South baselines including telescopes in Chile (e.g., ALMA) or Mexico (LMT) (see Figure 2). These are also the telescopes with the greatest ability to distinguish between and test the various models. Adding a nearly orthogonal baseline orientation allows a probe of the 2D structure of the image. There is also a signature of the shadow in the closure phase [17], and combining amplitude and phase information probably offers the best chance for its detection.

5. Variability

These radiative models are the first to self-consistently include variability from first principles. The variability in the accretion disk emission is driven by fluctuations in the particle density and magnetic field strength, which in turn are caused by magnetic turbulence driven by the MRI [37]. These fluctuations are highly correlated with those in the accretion rate, although the power law index of the power spectrum differs between the two quantities [47, 17].

6. Discussion

We have discussed the first models of the event horizon scale millimeter-wavelength emission in Sgr A* and M87 from 3D GRMHD simulations. The models are constructed by performing general relativistic radiative transfer on the simulation data via ray tracing, and can then be used to compare to or make predictions for mm-VLBI observations. Even with limited data, the observations are able to constrain the viewing geometry and physical conditions in the Sgr A* accretion flow. Thus far, the uncertainties in the parameter estimates decrease, while the values remain consistent, as more mm-VLBI data become available. For M87, we predict a size of 33 – 44 μ as, where within that range the size depends on the total millimeter flux of the source at the time of observation, whether the emission comes from a disk or jet, and on the viewing geometry within the allowed range. In both sources, the variability from the models agrees with observations, especially in Sgr A* where even the morphology of the millimeter flares can be reproduced with no additional free parameters. In both sources, the black hole shadow, a signature of the event horizon, may be accessible to future mm-VLBI observations using ALMA and/or the LMT.

6.1. Uncertainties

The results presented here apply to existing simulations with modest disk scale heights ($H/R \simeq 0.2$) at relatively high black hole spins ($a \simeq 0.5 - 0.9375$) where the black hole spin and accretion disk angular momentum axes are aligned. We expect the accretion flow in low-luminosity sources should be somewhat thicker ($H/R \simeq 1$). The first GRMHD simulations with $H/R \simeq 1$ have recently been carried out (McKinney et al., in preparation), and may be used to study both Sgr A* and M87. These simulations span a wide range of black hole spin and initial magnetic field configuration, and will allow a fairly robust parameter study of these radiative models including estimates of all relevant parameters including the black hole spin.

For the accretion disk component, a constant ratio of T_i/T_e is assumed with no justification. This assumption may be okay, since the millimeter emission region in these sources is so compact that their physical conditions do not vary greatly. However, this approximation should be tested in the future.

The primary uncertainty in the jet modeling is the dissipation physics and jet mass loading, both of which are important for constructing images. When the emission region is compact ($R \lesssim 5M$), relativistic effects tend to shape the images into crescents for a large range of emission geometries. The jet emission region may be extended, however, in which case most of the results for jet images discussed here for 1.3mm do not apply. This is true observationally for M87 at 7mm. We have assumed the non-thermal particle density is proportional to the magnetic energy density, but other sub-grid prescriptions should be tried as well, if only to gauge the range of viable jet image morphologies.

Finally, in geometrically thick sources the accretion flow and black hole spin orientations are likely to remain misaligned. This disk “tilt” has drastic consequences for the structure and evolution of the accretion flow [19, 48, 49] and its observational properties [50]. The conclusions reached here regarding crescent images, the visibility of black hole shadows, and variability driven by MRI turbulence all apparently hold for similar models from simulations with a 15° tilt [14]. However, the parameter estimates for Sgr A* discussed above only apply in the aligned case.

Acknowledgments

This work was partially supported by NASA Earth & Space Science Fellowship NNX08AX59H (JD), STScI grant HST-GO-11732.02-A, NSF grant AST 0807385, NASA grant 05-ATP05-96, and NASA Chandra Fellowship PF7-80048 (JCM).

References

- [1] Balick B and Brown R L 1974 ApJ **194** 265–270
- [2] Doeleman S S, Weintroub J, Rogers A E E, Plambeck R, Freund R, Tilanus R P J, Friberg P, Ziurys L M, Moran J M, Corey B, Young K H, Smythe D L, Titus M, Marrone D P, Cappallo R J, Bock D C J, Bower G C, Chamberlin R, Davis G R, Krichbaum T P, Lamb J, Maness H, Niell A E, Roy A, Strittmatter P, Werthimer D, Whitney A R and Woody D 2008 Nature **455** 78–80 (*Preprint* 0809.2442)
- [3] Fish V L, Doeleman S S, Beaudoin C, Blundell R, Bolin D E, Bower G C, Chamberlin R, Freund R, Friberg P, Gurwell M A, Honma M, Inoue M, Krichbaum T P, Lamb J, Marrone D P, Moran J M, Oyama T, Plambeck R, Primiani R, Rogers A E E, Smythe D L, SooHoo J, Strittmatter P, Tilanus R P J, Titus M, Weintroub J, Wright M, Woody D, Young K H and Ziurys L M 2011 ApJ **727** L36+ (*Preprint* 1011.2472)
- [4] Yuan F, Quataert E and Narayan R 2003 ApJ **598** 301–312 (*Preprint* arXiv:astro-ph/0304125)
- [5] Broderick A E, Fish V L, Doeleman S S and Loeb A 2009 ApJ **697** 45–54 (*Preprint* 0809.4490)
- [6] Broderick A E, Fish V L, Doeleman S S and Loeb A 2011 ApJ **735** 110+ (*Preprint* 1011.2770)
- [7] Balbus S A and Hawley J F 1991 ApJ **376** 214–233
- [8] Goldston J E, Quataert E and Igumenshchev I V 2005 ApJ **621** 785–792 (*Preprint* arXiv:astro-ph/0411627)
- [9] Noble S C, Leung P K, Gammie C F and Book L G 2007 *Class. and Quant. Gravity* **24** 259+ (*Preprint* arXiv:astro-ph/0701778)
- [10] Mościbrodzka M, Gammie C F, Dolence J C, Shiokawa H and Leung P K 2009 ApJ **706** 497–507 (*Preprint* 0909.5431)

- [11] Shcherbakov R V, Penna R F and McKinney J C 2010 *ArXiv e-prints (Preprint 1007.4832)*
- [12] Mościbrodzka M, Gammie C F, Dolence J C and Shiokawa H 2011 *ApJ* **735** 9+ (*Preprint 1104.2042*)
- [13] Hilburn G and Liang E 2011 *ArXiv e-prints (Preprint 1109.2847)*
- [14] Dexter J 2011 *Radiative Models of Sagittarius A* and M87 from Relativistic MHD Simulations* Ph.D. thesis University of Washington
- [15] Luminet J P 1979 *A&A* **75** 228–235
- [16] Drappeau S, Dibi S, Dexter J, Markoff S and Fragile P C 2011 Self-consistent spectra from GRMHD simulations with radiative cooling: A link to reality for Sgr A *SF2A-2011: Proceedings of the Annual meeting of the French Society of Astronomy and Astrophysics* ed G Alecian, K Belkacem, R Samadi, & D Valls-Gabaud pp 563–565
- [17] Dexter J, Agol E, Fragile P C and McKinney J C 2010 *ApJ* **717** 1092–1104 (*Preprint 1005.4062*)
- [18] Anninos P, Fragile P C and Salmonson J D 2005 *ApJ* **635** 723–740 (*Preprint arXiv:astro-ph/0509254*)
- [19] Fragile P C, Blaes O M, Anninos P and Salmonson J D 2007 *ApJ* **668** 417–429 (*Preprint 0706.4303*)
- [20] Fragile P C, Lindner C C, Anninos P and Salmonson J D 2009 *ApJ* **691** 482–494 (*Preprint 0809.3819*)
- [21] Gammie C F, McKinney J C and Tóth G 2003 *ApJ* **589** 444–457 (*Preprint arXiv:astro-ph/0301509*)
- [22] Noble S C, Gammie C F, McKinney J C and Del Zanna L 2006 *ApJ* **641** 626–637 (*Preprint arXiv:astro-ph/0512420*)
- [23] McKinney J C 2006 *MNRAS* **367** 1797–1807 (*Preprint arXiv:astro-ph/0601410*)
- [24] Tchekhovskoy A, McKinney J C and Narayan R 2007 *MNRAS* **379** 469–497 (*Preprint 0704.2608*)
- [25] McKinney J C and Blandford R D 2009 *MNRAS* **394** L126–L130 (*Preprint 0812.1060*)
- [26] Narayan R and Yi I 1994 *ApJ* **428** L13–L16 (*Preprint arXiv:astro-ph/9403052*)
- [27] Falcke H and Markoff S 2000 *A&A* **362** 113–118 (*Preprint arXiv:astro-ph/0102186*)
- [28] Ly C, Walker R C and Wrobel J M 2004 *AJ* **127** 119–124 (*Preprint arXiv:astro-ph/0309743*)
- [29] Walker R C, Ly C, Junor W and Hardee P J 2008 *Journal of Physics Conference Series* **131** 012053–+
- [30] Dexter J, McKinney J C and Agol E 2011 *ArXiv e-prints (Preprint 1109.6011)*
- [31] Broderick A E and McKinney J C 2010 *ApJ* **725** 750–773 (*Preprint 1006.5015*)
- [32] Leung P K, Gammie C F and Noble S C 2011 *ApJ* **737** 21–+
- [33] Dexter J and Agol E 2009 *ApJ* **696** 1616–1629 (*Preprint 0903.0620*)
- [34] Fragile P C and Anninos P 2005 *ApJ* **623** 347–361 (*Preprint arXiv:astro-ph/0403356*)
- [35] McKinney J C 2006 *MNRAS* **368** 1561–1582 (*Preprint arXiv:astro-ph/0603045*)
- [36] Marrone D P 2006 *Submillimeter properties of Sagittarius A*: The polarization and spectrum from 230 to 690 GHz and the submillimeter array polarimeter* Ph.D. thesis AA(Harvard University)
- [37] Dexter J, Agol E and Fragile P C 2009 *ApJ* **703** L142–L146 (*Preprint 0909.0267*)
- [38] Agol E 2000 *ApJ* **538** L121–L124 (*Preprint arXiv:astro-ph/0005051*)
- [39] Quataert E and Gruzinov A 2000 *ApJ* **545** 842–846 (*Preprint arXiv:astro-ph/0004286*)
- [40] Marrone D P, Moran J M, Zhao J and Rao R 2007 *ApJ* **654** L57–L60 (*Preprint arXiv:astro-ph/0611791*)
- [41] Sparks W B, Biretta J A and Macchetto F 1996 *ApJ* **473** 254–+
- [42] Perlman E S, Biretta J A, Sparks W B, Macchetto F D and Leahy J P 2001 *ApJ* **551** 206–222 (*Preprint arXiv:astro-ph/0012044*)
- [43] Perlman E S, Mason R E, Packham C, Levenson N A, Elitzur M, Schaefer J J, Imanishi M, Sparks W B and Radomski J 2007 *ApJ* **663** 808–815 (*Preprint 0704.1156*)
- [44] Tan J C, Beuther H, Walter F and Blackman E G 2008 *ApJ* **689** 775–781
- [45] Bardeen J M 1973 Timelike and null geodesics in the Kerr metric. *Black holes (Les astres occlus)* ed DeWitt B S and DeWitt C (New York: Gordon and Breach) p 215
- [46] Falcke H, Melia F and Agol E 2000 *ApJ* **528** L13–L16 (*Preprint arXiv:astro-ph/9912263*)
- [47] Noble S C and Krolik J H 2009 *ApJ* **703** 964–975 (*Preprint 0907.1655*)
- [48] Fragile P C and Blaes O M 2008 *ApJ* **687** 757–766 (*Preprint 0807.2453*)
- [49] Fragile P C 2009 *ApJ* **706** L246–L250 (*Preprint 0910.5721*)
- [50] Dexter J and Fragile P C 2011 *ApJ* **730** 36–+ (*Preprint 1101.3783*)